Effects of interplay between metal subwavelength slits on extraordinary optical transmission*

Wei Fei-Fei(魏菲菲)[a], Wang Huai-Yu(王怀玉)[b]†, and Zhou Yun-Song(周云松)[a]‡

[a] *Department of Physics, Capital Normal University, Beijing* 100037, *China*
[b] *Department of Physics, Tsinghua University, Beijing* 100084, *China*

(Received 16 July 2012; revised manuscript received 29 August 2012)

In this paper we study the extraordinary optical transmission of one-dimensional multi-slits in an ideal metal film. The transmissivity is calculated as a function of various structural parameters. The transmissivity oscillates, with the period being just the light wavelength, as a function of the spacing between slits. As the number of slits increases, the transmissivity varies in one of three ways. It can increase, attenuate, or remain basically unchanged, depending on the spacing between slits. Each way is in an oscillatory manner. The slit interaction responsible for the oscillating transmission strength that depends on slit spacing is the subject of more detailed investigation. The interaction most intuitively manifests as a current distribution in the metal surface between slits. We find that this current is attenuated in an oscillating fashion from the slit corners to the center of the region between two adjacent slits, and we present a mathematical expression for its waveform.

Keywords: extraordinary optical transmission, metal subwavelength slits, interplay between slits

PACS: 42.15.Eq, 42.79.Dj, 78.68.+m **DOI:** 10.1088/1674-1056/22/2/024201

1. Introduction

The phenomenon of light falling on a metal grating structure has been studied for a long time, where the work by Lord Rayleigh[1,2] might be the most representative. Over the years, experimental techniques have been developed rapidly with scientific achievements. A new development was made in 1998 by Ebbesen *et al*.[3] who first discovered the extraordinary optical transmission (EOT) of a small aperture in a metal film. The experimental results showed that the transmissivity was very much greater than that expected by classical diffraction theory, and greater than the expected results in accordance with the occupied area ratio, and it showed that light could "couple" to the other side of a metal film in such a way that the light did not directly pass through the holes. Around that time, the EOT of metal film containing sub-wavelength slits with a grooved structure was studied, and it was found that the transmissivity depended on the film thickness, distance between the slits, and depth of the grooves.[4–7] As an extension, further research has been carried out to explore the EOT of more complex sub-wavelength structure and the interest in understanding the physics of the phenomena in order to find application of EOT in optical components was aroused.[8–21] Regarding the explanation of EOT, two theories have been suggested. It was proposed[3,10,11] that the incident beam activated surface plasmon polaritons (SPP) on the surface of the metal structure comprising a narrow slit, that the SPP coupled light into the slit, thereby enhancing the intensity of the light entering the slit, and that it also scattered the emergent light out of the cavity, resulting in an SPP resonance. Another explanation[22–26] postulated a resonance of a Fabry–Perot (F–P) cavity in which SPP standing waves were generated in the slit, so that the transmissivity of light of a specific frequency was enhanced as the light passed through the slit. In fact, these two theories did not contradict each other, because the real process of EOT involves the combination of these two aspects.[27,28]

Many metal structures that can exhibit EOT have been studied, such as the single-aperture[10] and single-slit structures,[8,15–17,26,29] the periodic slot arrays,[30–34] gratings,[35–39] double-slit structures,[40] etc. For a multi-aperture structure, the apertures have usually been considered as periodically arranged, such as a grating, for the convenience of investigation.

Practically, slits in metal films have never really been periodically arranged, since the number of slits in real components must be finite. To date, studies on the transmission of a finite number of slits have been rare, perhaps because the treatment of non-periodic structures is more complicated than that of periodic ones. The interaction between slits in a multi-slit structure is an interesting topic, however. In this paper, we study the transmissivity of an ideal non-periodic metal structure containing a finite number of slits. The transmissivities of structures with single and multi-slits are compared, and the factors that influence the transmissivity are analyzed. Particular attention is paid to the interaction between slits as it affects the transmissivity and is reflected by currents in the metal surface region between slits. The total current can be regarded

*Project supported by the National Natural Science Foundation of China (Grant Nos. 11074145, 10874124, and 61275028).
†Corresponding author. E-mail: wanghuaiyu@mail.tsinghua.edu.cn
‡Corresponding author. E-mail: 263zys@263.net
© 2013 Chinese Physical Society and IOP Publishing Ltd

as the superposition of currents emanating from the slits, and its waveform can be described by an equation. The information inferred from this study may be useful in preparing subwavelength metal multi-slit structures for experiments.

2. Model and method

The structural model is depicted in Fig. 1. The metal film is an ideal conductor, and extends infinitely in the xy plane, with thickness w along the z direction. There are N identical slits equally spaced along the x direction. The width of each slit is a, and the slit length is equal to the film's thickness w. The spacing between adjacent slits is denoted as b. A monochromatic plane wave with frequency ω is vertically incident on the metal film along the z direction, with its magnetic field parallel to the y axis. Maxwell's equation can be separated into two parts,[1] one with the electric field parallel to the y axis, describing s-polarized light, and the other with the magnetic field parallel to the y axis, i.e. p-polarized waves. In the following, we consider the case of the p-polarization, i.e., TM waves. Maxwell's equation reads

$$\nabla^2 H_y(\boldsymbol{r}) + \frac{\omega^2}{c^2} H_y(\boldsymbol{r}) = 0, \tag{1}$$

where $H_y(\boldsymbol{r})$ is the component of the magnetic field along the y direction, and $\boldsymbol{r} = (x, z)$. The magnetic fields in regions I and III are expressed by

$$H_y^{\mathrm{I}}(\boldsymbol{r}) = H_y^{\mathrm{inc}}(\boldsymbol{r}) + \int_{-\infty}^{+\infty} \mathrm{d}k\rho(k) \exp[\mathrm{i}(kx - k_z z)] \tag{2}$$

and

$$H_y^{\mathrm{III}}(\boldsymbol{r}) = \int_{-\infty}^{+\infty} \mathrm{d}k\tau(k) \exp[\mathrm{i}(kx + k_z z)], \tag{3}$$

respectively, where $H_y^{\mathrm{inc}}(r) = \exp(\mathrm{i}k_0 z)$ represents the incident field, k_0 is the incident wave vector, and $\rho(k)$ and $\tau(k)$ are the reflection coefficient and the transmission coefficient, respectively.

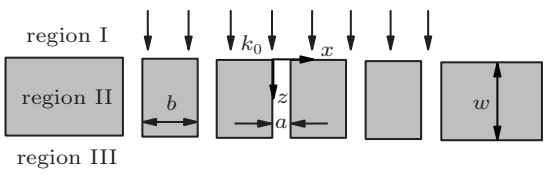


Fig. 1. Metal multi-slit structure consisting of subwavelength slits.

The magnetic field in the p-th slit in region II can be written as[29,30]

$$H_{py}^{\mathrm{II}}(r) = \sum_{m=0}^{\infty} [A_m \exp(\mathrm{i}\beta_m z) + B_m \exp(-\mathrm{i}\beta_m z)] \Phi_{pm}(x), \tag{4}$$

where $\beta_m = \sqrt{k_0^2\varepsilon - (m\pi/a)^2}$ and $\varepsilon = 1$. The wave function $\Phi_{pm}(x)$ is derived by solving Eq. (1) using the boundary conditions for the slit, and expressed as

$$\Phi_{pm}(x) = \sqrt{\frac{2}{Na}} \cos\frac{m\pi}{a}\left[x + \frac{a}{2} - p(a+b)\right],$$
$$p(a+b) - \frac{a}{2} \le x \le p(a+b) + \frac{a}{2}, \quad m = 1, 2, 3, \ldots, \tag{5}$$
$$p = -(N-1)/2, -(N-3)/2, \ldots, (N-3)/2, (N-1)/2,$$
$$\Phi_{p0}(x) = \frac{1}{\sqrt{Na}}. \tag{6}$$

Under the boundary conditions for the magnetic and electric fields at $z = 0$ and $z = w$, the reflection and transmission amplitudes A_m and B_m in the slits are solved from the simultaneous linear equations. More conveniently, two sets of quantities are defined by A_m and B_m as

$$E_m^{\mathrm{I}} = \frac{1}{k_0\varepsilon}\beta_m (A_m - B_m) \tag{7}$$

and

$$E_m^{\mathrm{O}} = \frac{1}{k_0\varepsilon}\beta_m [A_m \exp(\mathrm{i}\beta_m w) - B_m \exp(-\mathrm{i}\beta_m w)]. \tag{8}$$

Therefore, the reflection and transmission coefficients can be written as

$$\rho(k) = \delta(k) - \sum_{m=0}^{\infty} E_m^{\mathrm{I}} S_m(k), \tag{9}$$

and

$$\tau(k) = \exp(-\mathrm{i}k_z w) \sum_{m=0}^{\infty} E_m^{\mathrm{o}} S_m(k), \tag{10}$$

respectively, where

$$S_m = \frac{\int_{-\infty}^{+\infty} \mathrm{d}x \Phi_{pm}(x) \mathrm{e}^{-\mathrm{i}kx}}{2\pi\sqrt{1 - k^2/k_0^2}}. \tag{11}$$

Here the set of eigenfunctions of the multi-slit structure is more complicated than the single-slit case.[26]

Upon substitution of Eqs. (9) and (10) into Eqs. (2) and (3), the simultaneous linear equations for E_m^{I} and E_m^{O} are achieved as

$$(f_m + g_{mm})E_m^{\mathrm{I}} + \sum_{m' \ne m} g_{mm'} E_{m'}^{\mathrm{I}} + g_m^v E_m^{\mathrm{o}} = I_m \tag{12}$$

and

$$(f_m + g_{mm})E_m^{\mathrm{o}} + \sum_{m' \ne m} g_{mm'} E_{m'}^{\mathrm{o}} + g_m^v E_m^{\mathrm{I}} = 0, \tag{13}$$

where

$$f_m = \frac{k_0\varepsilon}{\beta_m} \frac{\exp(\mathrm{i}\beta_m W) + \exp(\mathrm{i}\beta_m W)}{\exp(-\mathrm{i}\beta_m W) - \exp(\mathrm{i}\beta_m W)}$$
$$= -\frac{k_0\varepsilon}{\mathrm{i}\beta_m} \cot(\beta_m W), \tag{14}$$
$$g_m^v = -\frac{k_0\varepsilon}{\beta_m} \frac{2}{\exp(\mathrm{i}\beta_m W) - \exp(-\mathrm{i}\beta_m W)}$$

$$= -\frac{k_0\varepsilon}{\mathrm{i}\beta_m \sin\beta_m W}, \tag{15}$$

$$g_{nm} = \int_{-\infty}^{+\infty} \mathrm{d}x\Phi_m(x) \int_{-\infty}^{+\infty} \mathrm{d}kS_m(k)\exp(\mathrm{i}kx), \tag{16}$$

and

$$I_m = 2\int_{-\infty}^{+\infty} \mathrm{d}x\Phi_m(x) = 2\sqrt{Na}\delta_{m0}. \tag{17}$$

The transmissivity is defined as

$$T = \frac{1}{Na}J_z = \frac{1}{Na}\int_{-\infty}^{+\infty} \mathrm{d}x\mathrm{Re}\left\{[\boldsymbol{E}^*(\boldsymbol{r})\times\boldsymbol{H}(\boldsymbol{r})]_z\right\}$$
$$= \frac{1}{Na}\mathrm{Re}\sum_{m,n=0}^{\infty} E_m^{\mathrm{O}*}E_n^{\mathrm{O}}g_{mn}. \tag{18}$$

Since a perfect metal is assumed, the electromagnetic waves cannot enter the metal. That is to say, the thickness of the surface current is zero. It is equivalent to having an infinite real positive dielectric constant. Therefore, the above fomula is applicable to any light wavelength.

3. Results and discussion

3.1. Double-slit structure

We first consider a double-slit as the simplest case in multi-slit structures.

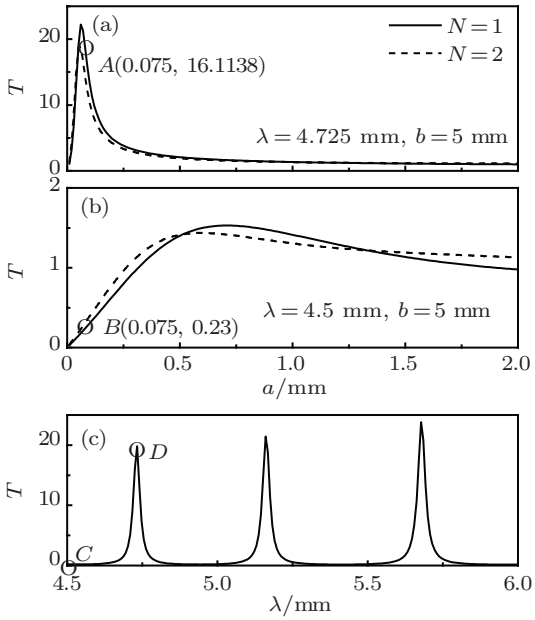


Fig. 2. Curves of transmissivity versus a for single-slit (solid line) and double-slit (dashed line) structures of film thickness $w = 28.2$ mm at (a) $\lambda = 4.725$ mm and (b) $\lambda = 4.5$ mm, with the spacing between slits of the double-slit structure being 5 mm. (c) Curve of transmissivity versus λ at $a = 0.075$ mm for a single-slit structure. Point A in panel (a) and point B in panel (b) are located on solid lines, and the corresponding wavelengths are marked by D and C, respectively, in Fig. 2(c).

Figure 2 shows the curves of the transmissivity as a function of slit width and light wavelength. When the slit width increases, the transmissivity first increases and then decreases as shown in Figs. 2(a) and 2(b). From the figure, it is evident that SPP acts as either enhancing or depressing the transmission of light through a sub-wavelength slit. When the slit width is fixed, the peak transmissivity occurs at particular wavelengths, as seen in Fig. 2(c).

The transmissivity varies remarkably with wavelength as shown by Points C and D in Fig. 2(c). It is well known that the EOT through a sub-wavelength slit is closely related to the FP interference of SPPs within the slit. For a fixed slit structure, transmissivity peaks will appear at particular wavelengths as shown in Fig. 2(c). Conversely, for a given wavelength, there will be only one transmissivity peak as a function of slit width as shown in Figs. 2(a) and 2(b).

Figure 3 shows the curves of T versus b for several slit numbers while other parameters are fixed. The horizontal solid line represents the transmissivity of a single-slit structure. The dashed line is that of a double-slit structure, and it oscillates periodically. The first four peaks appear at about $b = 2.81$, 7.54, 12.27, and 17.00 mm, respectively, showing that the period simply equals the wavelength, $\lambda = 4.73$ mm. Clearly, there is an interaction between the two slits, which is diminished as the spacing increases. This manifests the fact that as the spacing between the two slits increases, the transmissivity of the double-slit structure approaches that of the single-slit structure. Also note that the higher the transmissivity peak, the lower the values of the nearest minima are.

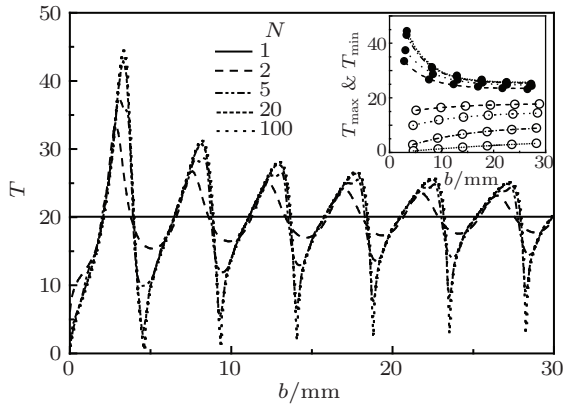


Fig. 3. Curves of transmissivity versus slit spacing b for multi-slits. Parameters are $a = 0.075$ mm, $w = 28.2$ mm, $\lambda = 4.725$ mm. Inset shows transmissivity maxima (solid circles) and minima (open circles) each as a function of slit spacing b.

The interaction between the slits can be more clearly understood by considering the surface current between them. This surface current is driven by electromagnetic waves and radiates energy into space, and this radiation loss increases when the slit spacing is extended. In a real metal, such a surface current penetrates the metal somewhat, in accordance with the skin effect, so that the current exists within some thickness in the metal.[21] Therefore, an additional energy drain is present by the Joule effect in addition to the radiation loss. In the present model, however, the metal is regarded as being ideal, so that the surface current is within a

zero-width layer and there is only the radiation loss in action. The attenuation in an ideal metal is always less than that in a real metal. The decrease of transmissivity peak associated with the increase of slit spacing (Fig. 3) is solely the result of electromagnetic wave emission from the metal surface.

The dashed curve exhibits minima at particular slit spacings, e.g., a position close to $b = 5$ mm. At these spacings, interference between slits reduces the transmissivity. From Fig. 2(a) it follows that the transmissivity of the double-slit structure is smaller than that of the single-slit structure when the parameter a exceeds a certain value, because the slit spacing and wavelength used in Fig. 2(a) are near their minima for the dashed line in Fig. 3.

The peak and valley values of the transmissivity in Fig. 3 are denoted by $T_{\max}$ and $T_{\min}$, respectively. The inset of Fig. 3 shows the curves of $T_{\max}$ and $T_{\min}$ versus b. The two dashed curves descend and ascend exponentially, and each of them has a good fitting to the curves described by

$$T_{\max} = T_{\max 0} e^{-b/\alpha_1} + c_1, \tag{19}$$

and

$$T_{\min} = T_{\min 0} e^{-b/\alpha_2} + c_2. \tag{20}$$

The parameters in these expressions are listed in Table 1.

Table 1. Parameters in Eqs. (19) and (20) at several values of slit number N.

N	$T_{\max 0}$	$T_{\min 0}$	α_1	α_2	c_1	c_2
2	18.34	–4.30	0.21	0.10	23.37	17.95
5	23.65	–7.68	0.20	0.10	24.61	14.88
20	36.58	–10.14	0.22	0.08	25.32	9.79
100	40.76	–6.46	0.23	0.03	25.60	6.25

3.2. Coupling effect between slits

Figures 4(a) and 4(b) show the distributions of magnetic fields between the two slits. The current in the metal surface between the slits is proportional to the magnetic field value. Therefore, figure 4 also illustrates the distribution of surface current densities. Stimulated currents occur at each slit and propagate outwardly along the metal surface. The current between the slits oscillates periodically, since it is produced by an alternating magnetic field. The oscillation period number between adjacent slits is determined by the ratio of b/λ. For example, in Fig. 4(a), the period numbers of the solid and dashed lines are less than 1 since their $b/\lambda < 1$, and the period number of the dotted line is greater than 1 since its $b/\lambda > 1$; in Fig. 4(b), the period numbers of the solid and dashed lines are between 4 and 5 since their b/λ values are between 4 and 5, and the period number of the dotted line is greater than 5 since its $b/\lambda > 5$. Due to structural symmetry, the waves generated by the two slits are symmetric with respect to the central line of the structure, and so is the superimposed waveform. Because of radiation loss, the amplitude decays with the distance from each of the two sides. As the spacing between slits increases, the amplitude of the entire waveform decreases.

As can be seen in Fig. 4(a), between the two slits, there is only one minimum but no maximum for the solid line. Two minima and one maximum appear on the dotted line. The solid line corresponds to the position $b = 3$ mm on the dashed line in Fig. 3, while the dotted line in Fig. 4(a) corresponds to the minimum for the position $b = 5$ mm at the dashed line in Fig. 3, just beside $b = 3$ mm. In Fig. 4(a), as the spacing between slits increases, the oscillating current in the metal surface between adjacent slits exhibits another maximum and minimum, i.e., an additional period appears. The curves in Fig. 4(b) demonstrate the same sort of phenomenon.

Figures 4(a) and 4(b) show the results of perfect metal. To compare the results of real metals, we simulate the distribution of magnetic fields at the surface of silver for an $N = 2$ structure by use of the finite-difference time-domain (FDTD) method.[28] The dielectric constant of Ag corresponding to light wavelength is taken from Ref. [28]. The result is shown in Fig. 4(c). There are some differences between the ideal and real metals. For example, there is a finite thickness for an electromagnetic wave to enter the real metal, and the magnetic field on the real metal surface is not simply the electric current in the surface. However, it is seen by comparing Fig. 4(b) with Fig. 4(c) that the magnetization distributions on the surfaces of ideal and real metals are the same in essence.

Figures 4(a) and 4(b) display that the number of oscillation periods of the current between slits increases as spacing augments. The current between slits is always symmetric with respect to the center, and reaches the maximum on the slit corner. Thus, it is deduced that the current is the superposition of attenuating waves emanating from the edges of the slit openings on both sides. For the surface region of the metal film between the slits we can write a simple expression to describe the waveform. One slit emits a cosine wave with an amplitude that is exponentially attenuated with distance, and the cosine wave is given as

$$j = j_0 e^{x/\gamma} \cos(qx + \varphi). \tag{21}$$

Given the symmetry of the double-slit structure, the magnetic field curves between the slits in Figs. 4(a) and 4(b) can be fitted by

$$j = j_0[e^{x/\gamma}\cos(qx + \varphi) + e^{-x/\gamma}\cos(qx - \varphi)], \tag{22}$$

where

$$-b/2 < x < b/2.$$

Some fitting parameter values for this expression are listed in Table 2.

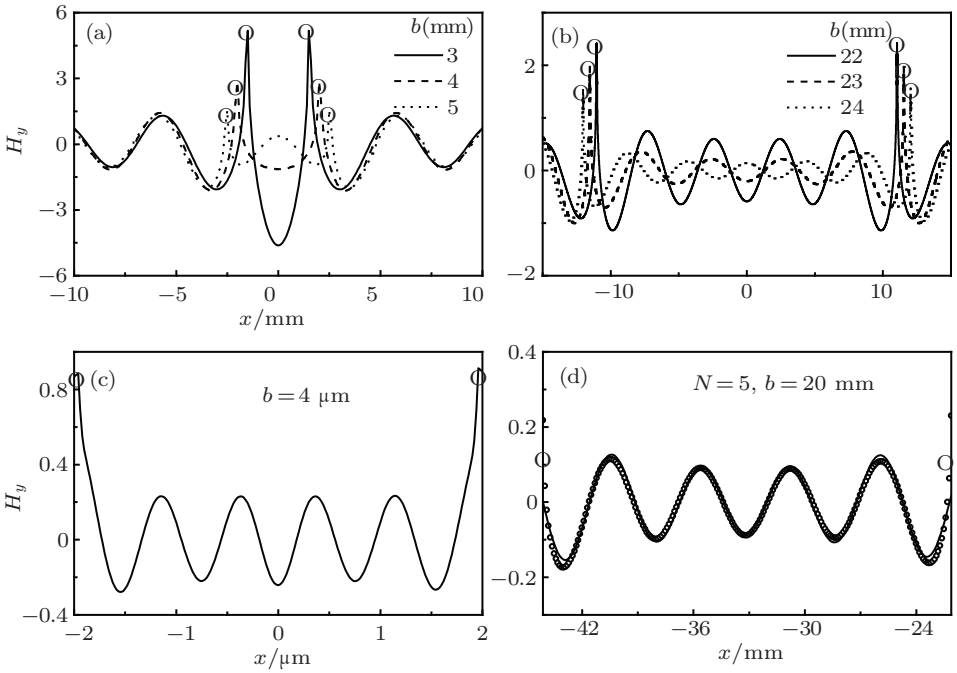


Fig. 4. Distributions of magnetic fields in front metal surface between the first and second slits when $\lambda = 4.725$ mm, $a = 0.075$ mm, $w = 28.2$ mm. (a) Ideal metal. $N = 2$, $b = 3$, 4, 5 mm; (b) Ideal metal. $N = 2$, $b = 22$, 23, 24 mm; (c) Real metal. $N = 2$, $\lambda = 0.8$ μm, $a = 0.1$ μm, $w = 0.1$ μm, $b = 4$ μm; (d) Ideal metal. $N = 5$, $b = 20$ mm. The larger open circles mark the location on the corner of the slit opening. In panels (a) and (b), the fitting curves are identical to the curves here so they are not plotted. In panel (d) the small open circles represent the calculated results and the solid line refers to the fitting curve.

Table 2. Parameters in Eq. (22) at several slit spacings.

b/mm	j_0	q	γ	φ
3	1.78	0.6	0.90	4.03
4	0.72	0.24	0.78	4.33
5	0.07	1.88	0.89	0.24
22	0.26	1.30	6.96	3.07
23	0.07	1.29	4.54	2.66
24	0.05	1.46	4.08	6.11

We have used j_0 to denote the maximum value of magnetic field on the slit corner. The attenuation parameter γ does not increase monotonically with the increase of slit spacing, because a particular spacing corresponds to a specific number of oscillation periods. The parameter γ drops when the spacing b varies from 3 mm to 4 mm, but then rises again when b increases from 4 mm to 5 mm.

Figure 5 shows the plots of T versus w at fixed slit widths and wavelengths. The transmissivity varies periodically with film thickness increasing, where the period is half the incident wavelength. The resonance positions and peak values of transmissivities occur at the same thickness w for the single- and double-slit structures. Since the transmissivities are different between the two structures (Fig. 3), we may deduce that the spacing between slits merely influences the value of the transmissivity, but has no effect on the position of the transmissivity peak. The coupling between slits is merely due to the action of two surface currents on the back and front surfaces of the film, and is not influenced by the length of a single slit. This is because the resonance position is determined by the FP resonance in the slit. The particular spacing between slits can either enhance or reduce this coupling. Radiation loss in the slit contributes to transmission without affecting transmissivity.

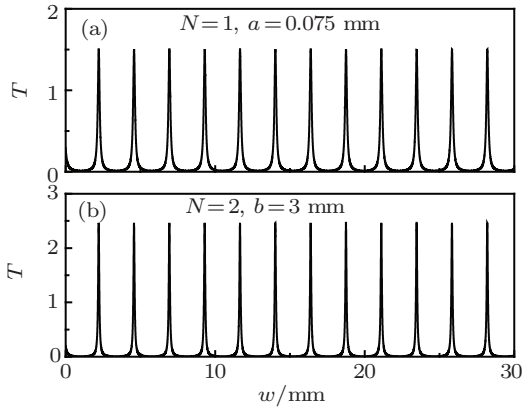


Fig. 5. Transmissivities of (a) single-slit and (b) double-slit structures each as a function of metal film thickness w. The wavelength and slit width are $\lambda = 4.725$ mm and $a = 0.075$ mm, respectively.

3.3. Multi-slit structure

With a knowledge of the details of the transmissivity of the double-slit structure, it is easy to understand the case of a multi-slit structure. Figure 3 shows how the transmissivities

vary with slit spacing for multi-slit structures with various slit numbers when $\lambda = 4.725$ mm.

Fix slit width and film thickness, then the transmissivity of a multi-slit structure will periodically oscillate and attenuate with the increase of slit spacing. The period is just the wavelength λ, independent of slit number. As the slit spacing increases, the transmissivity of a multi-slit structure approaches that of the single-slit structure. This indicates that the interaction between slits decreases, and for large spacings, slits will act nearly independently.

Evidently, the positions of the transmissivity extremum in the transmission curve for the multi-slit structure deviate from those of the two-slit structure, reflecting their structural discrepancies. As the slit number increases, the environment surrounding each slit changes, which affects EOT by the change in resonance position; what is more, the transmission curve is steeper for a larger number of slits, i.e., the transmissivity maximum becomes higher and the minimum becomes lower. When N is sufficiently large, the minimum transmissivity values can even become zero. For films with a greater number of slits, the coupling between all slits is enhanced even up to the point of total loss of transmissivity. The coupling between slits is related to the slit number, which reflects the effects of second adjacent and farther slits.

The maximum and minimum values in the transmissivity curves in Fig. 3 are plotted in the inset of that figure. All the descending curves in the inset can be fitted by Eq. (19) and all the ascending curves by Eq. (20). The fitting parameters are listed in Table 1. It is seen in Table 1 that $T_{\max 0}$, c_1, and c_2 vary monotonically with N, while the other three parameters do not. In a multi-slit structure, the interaction between additional slits adds complexity beyond what is found for the double-slit structure. As a consequence, the coefficients do not necessarily vary monotonically.

The transmissivity of multi-slit structures varies periodically with film thickness where the period is half the incident wavelength, exactly the same as the cases of single-slit and double-slit structures shown in Fig. 5, so they are not shown. It is inferred that the period of transmissivity variation as a function of slit spacing and film thickness is uniquely determined by the wavelength of the incident light. The transmissivity does not attenuate with film thickness increasing in the case of ideal conductors.

The open circles in Fig. 4(d) demonstrate the distribution of magnetic field between the first and second slits when $N = 5$ and $b = 20$ mm. All five slits, but for the central one, are not subject to symmetry. The solid line in Fig. 4(d) is a fitted curve, derived from the expression

$$j = j_{10}\,\mathrm{e}^{-(x+x_0)/a_1}\cos(q_1(x+x_0)+\varphi_1) + j_{20}\,\mathrm{e}^{(x+x_0)/a_2}\cos(q_2(x+x_0)-\varphi_2), \tag{23}$$

where $-b/2 < x < b/2$, $x_0 = 33.11$,

$$j_{10} = 0.46, \quad a_1 = 46.44, \quad q_1 = 1.2, \quad \varphi_1 = 89.65,$$
$$j_{20} = 0.47, \quad a_2 = 191.39, \quad q_2 = 1.2, \quad \varphi_2 = 89.61.$$

These parameters imply that the major cause of the asymmetry in the waveform in Fig. 4(d) is related to the difference in attenuation between the two components of the currents, i.e., a_1 and a_2 are different. On the other hand, the amplitudes, oscillation periods, and phases of these two current components are nearly the same, independent of the number of slits in the structure. The current between any two adjacent slits can be regarded as the superposition of two attenuating cosine waves, propagating in opposite directions. When the component currents propagate along the metal surface, they radiate electromagnetic waves into space, resulting in energy loss. Therefore, the amplitude of the waveform in Fig. 4(d) in the central position is lowest.

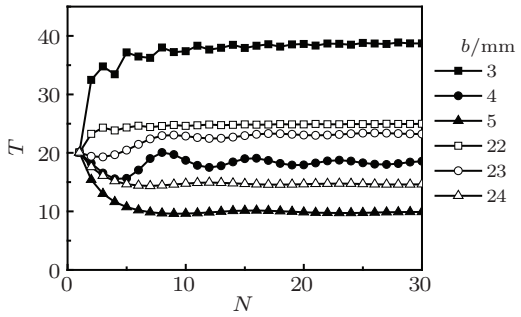


Fig. 6. T versus N at six b values with $w = 28.2$ mm, $a = 0.075$ mm, and $\lambda = 4.725$ mm. The solid lines are guides to the eyes.

Figure 6 shows plots of T versus N for several values of b with $w = 28.2$ mm, $a = 0.075$ mm, and $\lambda = 4.725$ mm. The three values of $b = 3$, 4, and 5 mm roughly correspond to a peak, medium and minimum transmissivity, respectively, of the curves in Fig. 3. It is remarkable that the transmissivity varies in three ways. When $b = 5$ mm, the transmissivity decreases with slit number increasing and eventually reaches a constant for large N. In this case, destructive interference between slits reduces the transmissivity. As N increases, the transmissivity decreases rapidly for low N, and then slowly with higher slit number. When N is small, the interaction between additional slits greatly affects transmissivity, while for large N, the multi-slit metal structure resembles a grating structure, with the transmissivity reaching a constant. When $b = 3$ mm, the transmissivity of the multi-slit structure exceeds that of a single-slit structure, and the transmissivity

curve slightly oscillates with N increasing and approaches a constant for large N. This indicates that constructive interference between slits enhances the transmissivity. When N is small, the environment near any slit is unique, and each additional slit greatly affects the transmissivity of all other slits, resulting in the slight oscillation of the overall transmissivity. Finally, when $b = 4$ mm, the transmissivity periodically oscillates with N and also approaches a constant. At this spacing, interference between slits does not particularly enhance or depress the transmissivity. Similar to the solid symbols for $b = 3$, 4, and 5 mm, the peaks, median values, and valleys of the transmissivity appear at $b = 22$, 23, and 24 mm, respectively, in Fig. 3, and are depicted by open symbols in Fig. 6. This figure again reflects the fact that the greater spacing between slits results in transmissivity that is closer to that of the single-slit structure.

Finally, a discussion about the difference between the multi-slit structures studied in this paper and traditional gratings is carried out. For traditional gratings, far-field detection is important, wherein the light arriving at a detector may be considered as a plane wave. At any observing point in the far field, light consists of the superposition of plane waves with fixed phase differences, which are determined by the observation angle. Therefore, the effects of destructive and constructive interference will appear on an observing screen. On the contrary, in this paper we present a study of the distribution of near-field light, where the observation point is just in the back surface of a metal film, or at the end of a slit. Therefore, the light waves at the observing point cannot be regarded as the superposition of plane waves, and the concepts of fixed phase and interference do not apply to such a scenario. Although figure 3 depicts peaks and valleys in the transmissivity curves, they do not belong in the interference phenomena related to gratings that are commonly mentioned in textbooks.

4. Conclusion

We investigated the transmittance properties of multi-slit metal structures, and the variation of the transmissivity as a function of slit width, slit spacing, slit length, and the number of slits. We first performed a detailed comparison of the transmissivity between single-slit and double-slit structures, and subsequently between double-slit and multi-slit structures. Finally, we described the dependence of transmissivity on the number of slits in a metal film. The following conclusions are drawn.

The transmissivity varies in an oscillating way as a function of slit spacing as well as the slit length. The oscillation period is determined by the incident light wavelength.

The peak value of the transmissivity decreases as the slit spacing increases. The attenuation is independent of the film thickness in the present case, since energy is not dissipated in an ideal conductor. As the slit spacing increases, the energy loss caused by the currents in the metal surface lowers the transmissivity.

In the metal surface between the corners of the adjacent two slits, electric currents are distributed in the way described by a cosine function, consisting of two wave components emitted from each of the corners, both exponentially decaying with distance from the corner. The current reaches a maximum at the slit corner, and attenuates near the center of the region between slits. The simulation results of the surface magnetic field of a two-slit structure made of real metal show the same feature.

The variation of transmissivity as a function of the number of slits is closely related to the slit spacing, and can take place in three possible forms: a) it decreases with number of metal slits increasing, b) it augments with the number of metal slits increasing, with slight oscillations, or c) it periodically oscillates with an increasing number of metal slits.

To summarize, the transmissivity of a multi-slit structure can be modified by adjusting slit spacing and the number of slits that make up the arrangement.

References

[1] Petit R 1908 *Electromagnetic Theory of Gratings* (Berlin: Springer)
[2] Sheng S, Stepleman R S and Sanda P N 1982 *Phys. Rev.* B **26** 2907
[3] Ebbesen T W, Lezec H J, Ghaemi H F, Thio T and Wolff P A 1998 *Nature* **391** 667
[4] Garcia-Vidal F J and Pendry J B 1996 *Phys. Rev. Lett.* **77** 1163
[5] Porto J A, Garcia-Vidal F J and Pendry J B 1999 *Phys. Rev. Lett.* **83** 2845
[6] Martin-Moreno L, Garcia-Vidal F J, Lezec H J, Degiron A and Ebbesen T W 2003 *Phys. Rev. Lett.* **90** 167401
[7] Garcia-Vidal F J, Lezec H J, Ebbesen T W and Martin-Moreno L 2003 *Phys. Rev. Lett.* **90** 213901
[8] Yang F and Sambles J R 2002 *Phys. Rev. Lett.* **89** 063901
[9] Lalanne P, Hugonin J P and Rodier J C 2005 *Phys. Rev. Lett.* **95** 263902
[10] Genet C and Ebbesen T W 2007 *Nature* **445** 39
[11] Liu H and Lalanne P 2008 *Nature* **452** 728
[12] Sturman B, Podivilov E and Gorkunov M 2010 *Phys. Rev.* B **82** 115419
[13] Wang B and Lalanne P 2010 *J. Opt. Soc. Am.* A **27** 1432
[14] Zhou L, Huang C, Wu S, Yin X, Wang Y, Wang Q and Zhu Y 2010 *Appl. Phys. Lett.* **97** 011905
[15] Babuty A, Bousseksou A, Tetienne J P, Moldovan D I, Sirtori C, Beaudoin G, Sagnes I, Wilde Y D and Colombelli R 2010 *Phys. Rev. Lett.* **104** 226806
[16] Zhou Y S, Gu B Y and Wang H Y 2010 *Phys. Rev.* A **81** 015801
[17] Bozhevolnyi S I 2001 *Phys. Rev. Lett.* **86** 3008
[18] Tian H, Liu J W, Qiu K, Song J and Wang D J 2012 *Chin. Phys.* B **21** 098504
[19] Tang T J, Zhou F and Li Y 2012 *Chin. Phys.* B **21** 064201
[20] Bashir Ahmed Tahira, Rashid Ahmedb, Ashiqa M G B, Afaq Ahmedc and Saeeda M A 2012 *Chin. Phys.* B **21** 044201
[21] Song D L, Chang J, Wang Q F, He W B and Cao Jiao 2011 *Chin. Phys.* B **20** 074201
[22] Takakura Y 2001 *Phys. Rev. Lett.* **86** 5601
[23] Yang F Z and Sambles J R 2002 *Phys. Rev. Lett.* **89** 063901
[24] Yang F and Sambles J R 2002 *Appl. Phys. Lett.* **81** 2047

[25] Treacy M M J 2002 *Phys. Rev*. B **66** 195105
[26] Bravo-Abad J, Martin-Moreno L and Garcia-Vidal F J 2004 *Phys. Rev.* E **69** 026601
[27] Zhou Y S, Gu B Y, Wang H Y and Lan S 2009 *Europhys. Lett.* **85** 24005
[28] Zhou Y S, Gu B Y, Wang H Y and Lan S 2010 *Chin. Phys. Lett.* **27** 037801
[29] Cao Q and Lalanne P 2002 *Phys. Rev. Lett.* **88** 057403
[30] Koerkamp K J K, Enoch S, Segerink F B, Van Hulst N F and Kuipers L 2004 *Phys. Rev. Lett.* **92** 183901
[31] Dintinger J, Klein S, Bustos F, Barners W L and Ebbesen T W 2005 *Phys. Rev.* B **71** 035424
[32] Barnes W L, Murray W A, Dintinger J, Devaux E and Ebbesen T W 2004 *Phys. Rev. Lett.* **92** 107401
[33] Gordon R, Brolo A G, McKinnon A, Rajora A, Leathem B and Kavanagh K L 2004 *Phys. Rev. Lett.* **92** 037401
[34] Collin S, Vincent G, Haidar R, Bardou N, Rommeluere S and Pelouard J L 2010 *Phys. Rev. Lett.* **104** 027401
[35] Zheng G G, Jiang J L, Xian F L, Qiang H X, Wu H and Li X Y 2011 *Chin. Phys.* B **20** 094201
[36] Zhao H J, Peng Y J, Tan J, Liao C R, Li P and Peng X X 2009 *Chin. Phys.* B **18** 5326
[37] Nesterov M L, Martin-Cano D, Fernandez-Dominguez A I, Moreno E, Martin-Moreno L and Garcia-Vidal F J 2010 *Opt. Lett.* **35** 423
[38] Luo M, Liu Q H and Guo J 2010 *J. Opt. Soc. Am.* B **27** 560
[39] Ye Y Q and Jin Y 2009 *Phys. Rev.* E **80** 036606
[40] Zhou Y S, Gu B Y, Lan S and Zhao L M 2008 *Phys. Rev.* B **78** 081404